Glucagon dysfunction in the liver induces hyperplasia of PP cells and the production of glucagon and pancreatic polypeptide double-positive cells

Yuko Nakagawa[1)], Takuro Horii[2)], Ayako Fukunaka[1)], Takashi Sato[1)], Masaki Kobayashi[3)], Tadahiro Kitamura[3)], Yoshitaka Hayashi[4)], Takashi Nishimura[5)], Izuho Hatada[2)], and Yoshio Fujitani[1)*]

[1)] Laboratory of Developmental Biology and Metabolism, Institute for Molecular and Cellular Regulation (IMCR), Gunma University, Maebashi 371-8512, Japan

[2)] Laboratory of Genome Science, Biosignal Genome Resource Center, Institute for Molecular and Cellular Regulation, Gunma University, Maebashi 371-8512, Japan

[3)] Metabolic Signal Research Center, Institute for Molecular and Cellular Regulation, Gunma University, Maebashi 371-8512, Japan

[4)] Department of Endocrinology, Research Institute of Environmental Medicine, Nagoya University, Nagoya 464-8601, Japan

[5)] Laboratory of Metabolic Regulation and Genetics, Institute for Molecular and Cellular

17 Regulation, Gunma University, Maebashi 371-8512, Japan

18

19 ***Corresponding author**

20 **E-mail:** fujitani@gunma-u.ac.jp (YF)

21 **Short Title:** Regulation of PP-cell proliferation in response to glucagon dysfunction

22 **Key words:** pancreatic endocrine cell, α cell, pancreatic polypeptide (PP) cell, glucagon function

Abstract

Understanding the mechanisms that regulate cellular identity and proliferation is crucial for elucidating cellular functions. Under normal conditions, pancreatic endocrine cells express only a single hormone, and their numbers are tightly regulated. Contrary to this general principle, our study revealed a significant increase in glucagon (GCG) and pancreatic polypeptide (PP) double-positive cells (GCG^+ PP^+ double-positive cells), along with hyperplasia of both PP and α cells in proglucagon-deficient mice. Similarly, systemic glucagon receptor-deficient mice exhibited PP-cell hyperplasia and an increase in GCG^+ PP^+ double-positive cells, with enhanced PP-cell self-replication observed at 4 weeks and the appearance of GCG^+ PP^+ double-positive cells at 10 weeks. Liver-specific glucagon receptor-deficient mice induced similar effects, which were linked to hyperaminoacidemia. Elevated glutamine levels were found to promote GCG^+ PP^+ double-positive cell formation via mTOR signaling, suggesting a molecular mechanism driving pancreatic endocrine cell plasticity. Collectively, these findings indicate that increased plasma amino acid levels caused by impaired glucagon action in the liver promotes the proliferation of α cells and PP cells, and disturbs their cellular identity maintenance.

Introduction

Each organ in the body precisely regulates both the number and types of its cells, to ensure proper function. Similarly, the pancreatic islets, the endocrine component of the pancreas, maintain a delicate balance among four types of cells: α cells, β cells, δ cells, and pancreatic polypeptide (PP) cells. These cells respectively secrete glucagon (GCG), insulin (INS), somatostatin (SST), and PP, working synergistically to regulate nutrients homeostasis, including glucose [1, 2]. Disruptions in the regulation of cell proliferation or identity within the islets are closely linked to the onset of various diseases. For example, β-cell dysfunction or loss is a characteristic feature of type 1 and type 2 diabetes, resulting in insufficient insulin action [3, 4]. Conversely, the excessive proliferation of endocrine cells can result in endocrine neoplasms, which may impair normal pancreatic function and cause severe clinical complications [5, 6]. Understanding the molecular mechanisms underlying cell fate determination and proliferation is therefore essential for maintaining the normal regulation of pancreatic islet function.

One of the endocrine cells, α-cells, their own proliferation by secreting glucagon, which acts on the liver to modulate amino acid catabolism [7]. Consequently, mice lacking the proglucagon gene which encodes glucagon [8, 9] or glucagon receptor [10-13] exhibit a common

55 phenotype: enhanced α-cell proliferation and hyperplasia. Incidentally the proglucagon gene
56 encodes multiple proteins, including glucagon, glucagon-like peptide-1 (GLP-1) and others.
57 Although these proteins are derived from the same gene, they have distinct receptors. As a result,
58 proglucagon gene-deficient mice lack all the encoded proteins, leading not only to glucagon
59 dysfunction but also to dysfunction of GLP-1 and others. Hyperplastic α cells caused by glucagon
60 dysfunction have been reported to develop into glucagonomas over time, and to metastasize to
61 the liver [14-16]. The mechanism underlying α-cell hyperplasia in the context of glucagon action
62 deficiency is well characterized. Previous studies have shown that impaired glucagon signaling
63 in the liver induces α-cell hyperplasia [13, 17-23]. This phenomenon is triggered by increased
64 blood amino acid levels, particularly glutamine, owing to reduced amino acid uptake and
65 catabolism in the liver. Increased glutamine levels upregulate the glutamine transporter Slc38a5
66 in α cells, promoting enhanced glutamine uptake and subsequent activation of the mTOR pathway,
67 which is a key driver of α-cell hyperplasia [18-21]. Notably, treatment of hyperplastic α cells with
68 the mTOR inhibitor rapamycin inhibits amino acid-dependent α-cell replication, and facilitates
69 their transdifferentiation into β-like cells [18]. This suggests that glucagon deficiency may
70 enhance the plasticity of islet cells, enabling them to differentiate into other cell types. In addition

71 to α cells, an increase in cells expressing the *Ppy* gene, which encodes PP, has been reported in
72 glucagon activity-deficient mice [8, 23]. However, it remains unclear whether the number of PP
73 protein-expressing cells actually increases, and how this is associated with the increase in α cells.
74 We previously reported our analysis of *Ppy*-lineage cells by lineage tracing experiments
75 using *Ppy-Cre* mice [24]. We showed that approximately half of the α cells are derived from the
76 *Ppy* lineage, suggesting that about half of the α cells express the *Ppy* gene. Furthermore, we
77 utilized *Ppy*-DTA mice, in which the diphtheria toxin A fragment is specifically expressed in *Ppy*-
78 expressing cells, leading to their ablation. Interestingly, in the islets of these mice, not only were
79 PP cells completely depleted, but approximately 80% of the α cells were also lost. These findings
80 indicate that, under normal conditions, a substantial proportion of α cells express the *Ppy* gene,
81 even if they do not produce the PP protein. This suggests that α cells share certain properties with
82 PP cells. It is possible that the absence of PP protein expression in many α cells is regulated by a
83 mechanism that suppresses PP protein translation, thereby contributing to the maintenance of α-
84 cell identity.
85 Endocrine cells generally follow the "one cell, one hormone" principle, but some cells are
86 known to express multiple hormones. In particular, during the early stages of human fetal

87 development (8–15 weeks of gestation), hormone double-positive cells, which co-express
88 multiple hormones, are frequently observed [25]. However, as fetal development progresses to
89 later stages, the number of these cells decreases, suggesting that they represent an intermediate
90 stage in endocrine cell differentiation. It is also suggested that immature cells may temporarily
91 express multiple hormones during differentiation. Furthermore, in the mature pituitary glands of
92 both fish and mammals, multi-hormonal cells, which produce and secrete multiple hormones
93 simultaneously, have been identified. In fish, these cells are thought to function to enable the
94 coordinated regulation of different hormones, which is necessary for adapting to changes in the
95 aquatic environment [26]. Additionally, in the pancreatic islets of mature mice, it has been
96 reported that some *PPY*-expressing cells co-express *INS*, *GCG*, or *SST* [27]. These cells exhibit a
97 mixed phenotypic profile, combining characteristics of β cells, α cells, and δ cells, and their gene
98 expression profiles overlap with those of these endocrine cell types. Notably, under diabetic stress
99 conditions, PP cells have been suggested to possess the plasticity to acquire insulin-producing
100 capacity. However, the physiological significance of these multi-hormonal cells remains largely
101 unknown.

102 In this study, we demonstrate that the hyperplasia of PP cells and GCG and PP double-

103 positive cells (GCG^+ PP^+ double-positive cells) occurs in proglucagon-deficient mice. We aimed

104 to identify the proteins encoded by the proglucagon gene that are responsible for inducing PP-cell

105 hyperplasia and the increase in GCG^+ PP^+ double-positive cells, as well as to elucidate the

106 underlying mechanisms.

Materials and methods

Animal care

The protocol for the animal experiments conducted in this study was formally approved by the Animal Care and Ethics Committee of Gunma University (approval number: D21-040). Mice were euthanized humanely by cervical dislocation following anesthesia with isoflurane (Fujifilm, Osaka, Japan), which was administered via a rodent anesthesia inhalation system (NARCOBIT-E, Natsume Seisakusho Co., Ltd., Tokyo, Japan). All efforts were made to minimize suffering. Mice were housed in a specific-pathogen-free barrier facility, maintained under a 12-hour light/dark cycle, and provided with unrestricted access to standard rodent chow (Oriental Yeast, Tokyo, Japan) and water.

Mice

B6D2F1 mice were purchased from CLEA Japan (Kawasaki, Japan), ICR mice were obtained from Charles River Japan (Yokohama, Japan), and C57BL/6JmsSlc mice were obtained from Japan SLC, Inc. (Shizuoka, Japan).

123 **Generation of *glucagon receptor* gene (*Gcgr*)-floxed mice**

124 *Gcgr*-floxed mice were generated by the sequential electroporation method that we reported
125 previously [28]. Sequences of target crRNAs flanking exons 4 to 13 of the *Gcgr* gene, and
126 corresponding donor single-stranded oligodeoxynucleotides including loxP are shown in Table 1.
127 Fertilized eggs were isolated from superovulated B6D2F1 female mice, 21 h post administration
128 of human chorionic gonadotropin (hCG). The first electroporation to insert the 5′ loxP into intron
129 3 was conducted at the 1-cell stage (24–26 h post hCG); and the second electroporation to insert
130 the 3′ loxP to intron 13 was conducted at the 2-cell stage (42–44 h post hCG). The sequentially
131 electroporated embryos were then transferred to the oviducts of pseudopregnant ICR females. The
132 floxed alleles of the obtained mice were confirmed by sequencing analysis. For PCR-based
133 confirmation, the primers used for each Flox insertion site were as follows: for the left Flox
134 insertion site, the forward primer was 5′-CTTGAAGGAGAGGTGCCTTG-3′, and the reverse
135 primer was 5′-GGCCAGCAGGAGTACTTGTC-3′, and a 268-bp band is detected. For the right
136 Flox insertion site, the forward primer was 5′-TCTTTCTCCAGGGTCTGCTG-3′, and the reverse
137 primer was 5′-CAAGTTTCACCTTGGGTTCA-3′, and a 250-bp band is detected.

138

139 **Generation of systemic *Gcgr*-knockout mice and liver-specific *Gcgr*-deficient mice**

140 The Cytomegalovirus (CMV) early enhancer and chicken β-actin (CAG) promoter -Cre

141 transgenic mice (*CAG-Cre*) [29, 30] were crossed with *Gcgr*-floxed mice. To confirm the

142 deletion of exon 4 to exon 13 in the *Gcgr* gene by Cre recombinase, PCR was conducted using

143 the following primers: 5′-CTTGAAGGAGAGGTGCCTTG-3′, and 5′-

144 CAAGTTTCACCTTGGGTTCA-3′. If the deletion is present, a 155-bp PCR product was

145 detected. Liver-specific glucagon receptor-knockout mice were generated by breeding *Gcgr*-

146 floxed mice and with albumin-*Cre* mice [31].

147

148 **Immunohistochemistry**

149 After anesthesia with isoflurane (Fujifilm, Osaka, Japan), mice were perfused with normal

150 saline through the heart to remove blood cells from the blood vessels. Subsequently, they were

151 perfusion-fixed with 4% paraformaldehyde (PFA), and their pancreata were harvested. The

152 harvested pancreata were fixed in 4% PFA at 4 °C overnight. Subsequently, the pancreata were

153 transferred to 70% ethanol. The pancreas samples were embedded in paraffin, and the paraffin

154 pancreas blocks were sectioned at a thickness of 5 μm, and subjected to immunostaining.

155 Immunofluorescence staining was conducted following previously described methods [32]. The
156 primary antibodies used were guinea pig anti-insulin (Ready-to-use, IR002, Dako-Agilent, Santa
157 Clara, CA, USA), rabbit anti-glucagon (1:1,000, ab92517, Abcam, Cambridge, UK), rabbit anti-
158 Ki67 (1:200, ab16667, Abcam), rabbit anti-somatostatin (1:1,000, T-4103, Peninsula Laboratories,
159 San Mateo, CA, USA), rabbit anti-pS6 (1:200, 4858, Cell Signaling Technology, Danvers, MA,
160 USA), mouse anti-PP (1:1,000, 23-2D3, IBL, Gunma, Japan) [32], and chicken anti-GFP (1:1,000,
161 ab13970, Abcam). Tissue sections were incubated with the primary antibody, followed by a
162 secondary antibody (Alexa Fluor 488, ab150077, Abcam; A11001 and A11039, Thermo Fisher
163 Scientific, Waltham, MA, USA; Alexa Fluor 594, A11012 and A11005, Abcam; Alexa Fluor 647,
164 A31573 and A31571, Abcam, all used at 1:1,000) together with the nuclear dye 4′,6-diamidino-
165 2-phenylindole (DAPI, Dojindo Molecular Technologies, Kumamoto, Japan). The sections were
166 then visualized using an FV1000 confocal laser-scanning microscope (Olympus, Tokyo, Japan).
167

168 **Quantification of α- and PP-cell mass**

169 The quantification of α-cell mass and PP-cell mass was performed as previously described
170 [24, 33]. Nonpancreatic tissues were removed from the pancreas, and the pancreas was weighed

171 before fixation in 4% paraformaldehyde for 6-hour. To obtain longitudinal sections from the tail
172 to the head of the pancreas, the pancreas was embedded in paraffin, and paraffin blocks were
173 prepared. From the entire pancreas, 6 sections per mouse were collected at 200-μm intervals, and
174 immunostained with an anti-glucagon or anti-PP antibody. The immunostained samples were
175 analyzed using a BX-9000 microscope and the BZII analysis application software (Keyence
176 Corporation, Osaka, Japan). The relative cross-sectional areas of α cells or PP cells were
177 determined by dividing the cross-sectional area occupied by α cells or PP cells by the total cross-
178 sectional area of the tissue. The total α-cell mass or PP-cell mass in the pancreas was calculated
179 by multiplying the relative cross-sectional area of each cell type by the weight of the pancreas.
180 Pancreata from four animals in each group were analyzed to determine the α-cell or PP-cell mass.
181

182 **Islet culture**

183 Following previously reported methods, islets were isolated from 10 week-old mice [34].
184 The islets were collected using a micropipette under a dissection microscope, and cultured
185 overnight in Roswell Park Memorial Instistute (RPMI) -1640 medium (11875093, Thermo Fisher
186 Scientific) supplemented with 1% penicillin/streptomycin. Subsequently, 100 islets were placed

187 on a 24-well plate coated with Matrigel (Corning Incorporated, Corning, NY, USA), and cultured
188 for 4 days. Islets in the control group were cultured in RPMI-1640 medium without L-glutamine
189 (32404, Thermo Fisher Scientific) supplemented with 500 μM L-glutamine. Islets in the
190 glutamine group were cultured in the same medium supplemented with 3,250 μM L-glutamine.
191 After the culture period, the islets were fixed with 4% PFA, followed by treatment with 15% and
192 30% sucrose solutions. Finally, a frozen block was prepared using Optimal Cutting Temperature
193 (OCT) compound, and the block was cryosectioned [32].
194
195 **Mouse plasma collection**
196 Prior to blood collection, the mice were weighed, and blood glucose levels were measured
197 using the Glutest Neo Alpha blood glucose meter (Sanwa Kagaku Kenkyusho Co. Ltd., Aichi,
198 Japan). Blood was collected by cutting the tails of the mice, and using a microhematocrit
199 heparinized capillary tube (22-362566, Thermo Fisher Scientific). The collected blood was then
200 transferred to a 1.5-mL tube. Subsequently, the collected blood was centrifuged at 6,200 rpm for
201 more than 5 minutes, and the supernatant was transferred to a new 1.5-mL tube, and frozen using
202 liquid nitrogen.

203

204 **Metabolomics analysis**

205 Widely targeted metabolomics analysis was performed as previously described [35, 36].
206 Briefly, frozen samples in 1.5-mL plastic tubes were homogenized in 300 μL of cold methanol
207 using φ3-mm zirconia beads and a freeze crusher (TAITEC Corp., Saitama, Japan) at 41.6 Hz for
208 2 min. The homogenates were mixed with 200 μL of methanol, 200 μL of H_2O, and 200 μL of
209 $CHCl_3$, and vortexed for 20 min at room temperature. The samples were then centrifuged at
210 15,000 rpm (20,000 *g*) for 15 min at 4 ℃. The supernatant was mixed with 350 μL of H_2O,
211 vortexed for 10 min at room temperature, and centrifuged at 15,000 rpm for 15 min at 4 ℃. The
212 aqueous phase was collected and dried down using a vacuum concentrator. The samples were
213 redissolved in 2 mM ammonium bicarbonate (pH 8.0) containing 5% methanol, and analyzed by
214 LC-MS/MS.

215 Chromatographic separations in an Acquity UPLC H-Class System (Waters, Milord, MA,
216 USA) were carried out under reverse-phase conditions using an ACQUITY UPLC HSS T3
217 column (100 mm × 2.1 mm, 1.8-μm particles, Waters) and under HILIC conditions using an
218 ACQUITY UPLC BEH Amide column (100 mm × 2.1 mm, 1.7-μm particles, Waters). Ionized

219 compounds were detected using a Xevo TQD triple quadrupole mass spectrometer coupled with

220 an electrospray ionization source (Waters). The peak area of a target metabolite was analyzed

221 using MassLynx 4.1 software (Waters).

222

223 **Statistical analyses**

224 Statistical analyses were performed using GraphPad Prism version 9.1.1 software

225 (GraphPad Software, San Diego, CA, USA). Results are presented as the mean ± standard error

226 of the mean (SEM). Differences between two groups were assessed using a two-tailed unpaired

227 Student *t*-test, and comparisons among three or more groups were performed using one-way

228 ANOVA followed by the Tukey test. A *p*-value of less than 0.05 was regarded as indicating a

229 statistically significant difference between groups.

230 **Results**

231 **Induced hyperplasia of PP cells and formation of multi-hormonal cells in proglucagon gene-**

232 **deficient mice**

233 Proglucagon gene-deficient mice (*Gcg*$^{gfp/gfp}$) lack the production of all hormones encoded

234 by the proglucagon gene, including glucagon and GLP-1, owing to the knock-in of the *gfp* gene

235 into the proglucagon gene locus [8]. *Gcg*$^{gfp/gfp}$ mice are known to demonstrate α-cell hyperplasia

236 similar to other mice with glucagon signaling deficiencies [37]. In *Gcg*$^{gfp/gfp}$ mice, GFP is

237 expressed in cells that would normally produce glucagon. Furthermore, it has been reported that

238 the expression level of *Ppy* mRNA is significantly elevated in the pancreatic islets of these mice

239 [8, 23]. Based on this, we performed fluorescence immunostaining using our developed PP

240 antibody [32] to investigate PP protein dynamics**.** Fluorescence immunostaining was performed

241 on pancreatic islet sections from 40 week-old *Gcg*$^{gfp/gfp}$ mice. In these islets, in addition to α-cell

242 hyperplasia, PP-cell hyperplasia was observed (Fig 1A). Furthermore, many GFP^{+} PP^{+} double-

243 positive cells were detected. Since the expression level of *SST* mRNA was also elevated [8],

244 although not as prominently as *Ppy* mRNA, we conducted triple staining using antibodies for PP,

245 GFP, and SST**.** In the pancreatic islets of *Gcg*$^{gfp/gfp}$ mice, PP^{+} GFP^{+} SST^{+} triple-positive cells were

246 identified (Fig 1B). In contrast, no PP^+ GCG^+ SST^+ triple-positive cells were observed in the

247 pancreatic islets of *Gcg*$^{+/+}$ mice when triple staining was performed using antibodies for PP, GCG,

248 and SST. These findings suggest that the absence of proteins encoded by the proglucagon gene

249 induces PP-cell hyperplasia and the formation of multi-hormonal cells. As the proglucagon gene

250 encodes multiple hormones, including glucagon, it was unclear as to exactly which hormone

251 deficiency caused the induction of PP-cell hyperplasia and the production of multi-hormonal cells.

252

253 **Increased PP cells in glucagon receptor-deficient mice**

254 To test whether glucagon, one of the proteins encoded by the proglucagon gene, is involved

255 in the above effects, *CAG-Cre* mice were crossed with *Gcgr*-floxed mice to produce *Gcgr* KO

256 (*Gcgr*$^{\Delta/\Delta}$) mice (Fig 2A). We next investigated whether PP-cell hyperplasia and the production of

257 GCG^+ PP^+ double-positive cells occur in *Gcgr*$^{\Delta/\Delta}$ mice at 10 weeks of age. Compared to *Gcgr*$^{+/+}$

258 control mice, *Gcgr*$^{\Delta/\Delta}$ mice demonstrated substantial PP-cell hyperplasia, and the presence of

259 GCG^+ PP^+ double-positive cells (Fig 2B). Quantitative analysis demonstrated a significant

260 increase in both PP-cell mass and the ratio of GCG^+ PP^+ double-positive cells relative to GCG^+-

261 positive cells in *Gcgr*$^{\Delta/\Delta}$ mice compared with *Gcgr*$^{+/+}$ mice (Figs 2C and D). These findings suggest

262 that glucagon signaling deficiency induces PP-cell hyperplasia and the emergence of GCG^{+} PP^{+}

263 double-positive cells.

264

265 **Induction of PP-cell self-replication and an increase in GCG^{+} PP^{+} double-positive cells**

266 **owing to glucagon dysfunction**

267 In 10 week-old *Gcgr*$^{\Delta/\Delta}$ mice, an increase in PP-cell mass and a rise in GCG^{+} PP^{+} double-

268 positive cells were observed. To assess how these changes progress at earlier stages, we examined

269 *Gcgr*$^{\Delta/\Delta}$ mice at 4 weeks of age. The PP cell mass in 4 week-old *Gcgr*$^{\Delta/\Delta}$ mice was significantly

270 higher than that in *Gcgr*$^{+/+}$ mice (Fig 3A and B). However, unlike the comparison at 10 weeks of

271 age (Fig 2B, right panel), the number of GCG^{+} PP^{+} double-positive cells in 4 week-old *Gcgr*$^{\Delta/\Delta}$

272 mice was not markedly increased compared to the control *Gcgr*$^{+/+}$ mice (Fig 3A, lower right panel).

273 Therefore, we quantitatively compared the number of GCG^{+} PP^{+} double-positive cells in *Gcgr*$^{\Delta/\Delta}$

274 mice between 4 and 10 weeks of age. The data showed that at 4 weeks of age, the number of

275 GCG^{+} PP^{+} double-positive cells was comparable to that in the control group. In contrast, at 10

276 weeks of age, the number of GCG^{+} PP^{+} double-positive cells was significantly higher in *Gcgr*$^{\Delta/\Delta}$

277 mice than in the control group (Fig 3C and D). Additionally, the number of GCG^{+} PP^{+} double-

278 positive cells in 4 week-old *Gcgr*$^{\Delta/\Delta}$ mice was significantly lower than that in 10 week-old *Gcgr*$^{\Delta/\Delta}$

279 mice. However, since an increase in PP cell mass was observed at 4 weeks of age, the increase in

280 PP cell mass was considered to be owning to factors other than an increase in double-positive

281 cells. To investigate this possibility, we analyzed PP-cell self-proliferation. Costaining analysis

282 was performed using antibodies against the proliferation marker Ki67, PP, and GCG to investigate

283 whether PP-cell self-proliferation was induced. The results showed that the number of Ki67^{+} PP^{+}

284 GCG^{-} cells was significantly higher in *Gcgr*$^{\Delta/\Delta}$ mice than in *Gcgr*$^{+/+}$ mice (Figs 3E and F). These

285 findings suggest that PP-cell self-proliferation is enhanced in *Gcgr*$^{\Delta/\Delta}$ mice. Furthermore,

286 considering the temporal changes in PP-cell mass and the increase in GCG^{+} PP^{+} double-positive

287 cells, it is likely that at 4 weeks of age, the increase in PP-cell mass is primarily owning to the

288 enhanced self-replication of PP cells caused by glucagon dysfunction, and that the increase in

289 GCG^{+} PP^{+} double-positive cells subsequently becomes apparent at 10 weeks of age.

290

291 **Induction of PP-cell hyperplasia and an increase in GCG^{+} PP^{+} double-positive cells is caused**

292 **by glucagon dysfunction in the liver**

293 Next, the tissue responsible for the hyperplasia of PP cells and the increase in GCG^+ PP^+

294 double-positive cells resulting from glucagon dysfunction was investigated. Albumin-

295 *Cre;Gcgr*$^{f/f}$ (Alb-*Cre;Gcgr*$^{f/f}$) mice, lacking glucagon signaling specifically in the liver, which is

296 the primary site of glucagon action, were generated. As previously reported [13], 10 week-old

297 Alb-*Cre;Gcgr*$^{f/f}$ mice demonstrated increased α-cell mass (S1 Fig). In addition, an increase in

298 PP-cell mass and the presence of GCG^+ PP^+ double-positive cells were observed (Figs 4A–C).

299 Further investigation of 40 week-old Alb-*Cre;Gcgr*$^{f/f}$ mice demonstrated a more pronounced

300 increase in PP-cell mass (S2 Fig), as well as the presence of both GCG^+ PP^+ double-positive

301 cells (Fig 4D). Previous studies have reported that liver-specific glucagon dysfunction mice

302 exhibit α-cell hyperplasia. However, regarding β cells, while pancreatic enlargement

303 leads to an increase in total β-cell mass, β-cell mass per gram of pancreas and insulin

304 secretion levels remain unchanged compared to control mice [13]. In this study, PP and

305 INS double staining was performed using Alb-*Cre;Gcgr*$^{f/f}$ mice, revealing the presence

306 of PP^+ INS^+ double-positive cells, which were not observed in control mice (Fig 4E).

307 These results suggest that hepatic glucagon dysfunction drives PP-cell hyperplasia and

308 the emergence of GCG^+ PP^+ and INS^+ PP^+ double-positive cells.

309

310 **Induction of increased PP cell numbers and GCG$^+$ PP$^+$ double-positive cells owing to**

311 **hyperaminoacidemia**

312 Since impaired glucagon action in the liver has been reported to elevate blood amino acid

313 levels [18, 20, 21], we examined whether amino acid levels were altered in the *Gcgr*$^{\Delta/\Delta}$ and Alb-

314 *Cre;Gcgr*$^{f/f}$ mice used in this study by measuring plasma amino acid concentrations. As expected,

315 plasma amino acid levels, including glutamine, were significantly increased in 10 week-old

316 *Gcgr*$^{\Delta/\Delta}$ and Alb-*Cre;Gcgr*$^{f/f}$ mice compared with control mice (S3 and S4 Figs). Next, we

317 investigated whether the addition of large amounts of glutamine would increase the number of PP

318 cells in the pancreatic islets and promote the formation of GCG$^+$ PP$^+$ double-positive cells. (Fig

319 5A). When pancreatic islets were cultured with a high concentration of glutamine, the proportions

320 of GCG$^+$ positive and PP$^+$ positive cells in the islets were significantly increased (Figs 5B and C).

321 Moreover, the ratio of GCG$^+$ PP$^+$ double-positive cells among GCG$^+$ positive cells also increased

322 (Fig 5D). To determine whether the increase in GCG$^+$ PP$^+$ double-positive cells was mediated by

323 the mTOR pathway, we treated islets with the mTOR kinase inhibitor rapamycin. The glutamine-

324 induced increase in GCG$^+$ PP$^+$ double-positive cells was significantly suppressed by rapamycin

325 treatment (Figs 5E and F). These results suggest that the increased glutamine levels increase the

326 number of GCG^+ positive cells, PP^+ positive cells, and GCG^+ PP^+ double-positive cells in the

327 pancreatic islets via activation of the mTOR pathway. Finally, we investigated whether mTOR

328 was activated in GCG^+ PP^+ double-positive cells using tissues from *Gcgr*$^{\Delta/\Delta}$ mice. Consistent with

329 the results from isolated islets, GCG^+ PP^+ $pS6^+$ triple-positive cells were observed in these mice,

330 supporting the role of mTOR activation in the formation of GCG^+ PP^+ double-positive cells (S5

331 Fig).

332

333

334 **Discussion**

335 In this study, we investigated liver-specific glucagon receptor-deficient mice, to gain
336 additional insights into the effect of glucagon deficiency, beyond the previously reported
337 hyperplasia of α cells [10-13]. We found that impaired glucagon signaling in the liver also leads
338 to the hyperplasia of PP cells, and the emergence of GCG^+ PP^+ double-positive cells (Fig 4).
339 Additionally, we observed a significant increase in plasma amino acid levels in these mice
340 compared with the control groups (S3 Fig). Furthermore, when islets isolated from wild-type mice
341 were cultured with high concentrations of glutamine, one of the increased amino acids, we found
342 that the increase in PP cells and GCG^+ PP^+ double-positive cells is facilitated by activation of the
343 mTOR signaling pathway (Fig 5).

344 Previous studies have reported that expression of the *Ppy* gene is upregulated in
345 proglucagon-deficient and glucagon receptor-deficient mice [8, 23], however, whether PP protein
346 expression is indeed increased in these mice remained unclear. In this study, as shown in Fig. 2B,
347 we observed a significant increase in PP protein expression owing to glucagon signaling
348 insufficiency, accompanied by a marked increase in PP-cell mass (Fig 2C). Smith *et al.* reported
349 similar findings in their single-cell RNA sequencing study of islets from systemic glucagon

350 receptor-deficient mice, in which they found a significant increase in the PP-cell cluster in
351 addition to the α-cell cluster [23]. These results support the findings of our present study.
352 Regarding the mechanism underlying the increase in PP cells, as illustrated in Figs 3E and 3F
353 systemic glucagon receptor-deficient mice demonstrated a higher proportion of Ki67-positive
354 cells among PP^+ cells that were not stained with glucagon antibodies, compared with control wild-
355 type mice. The number of PP cells was also higher in the glucagon receptor-deficient mice than
356 in controls. These findings suggest that glucagon signaling insufficiency promotes an increase in
357 PP-cell mass through self-proliferation. The mechanism underlying PP-cell self-proliferation
358 remains unclear and represents a future research question. However, as shown in S6 Fig, in 4
359 week-old *Gcgr*$^{\Delta/\Delta}$ mice, pS6 signals were not detected in PP single-positive cells. This suggests
360 that a different pathway, distinct from the mechanism by which GCG^+ PP^+ double-positive cells
361 activate the mTOR signaling pathway to promote proliferation, may be involved. Previous studies
362 have reported that other pancreatic endocrine cells, such as α and δ cells, also demonstrate
363 enhanced proliferation under glucagon signaling deficiency, although the mechanisms differ. α
364 cells increase in number through self-proliferation [37], whereas δ cells expand through both self-
365 proliferation and duct-derived neogenesis [38]. In this study, we proposed that the increase in PP-

366 cell numbers is driven by both self-proliferation and an increase in multi-hormone-producing cells.

367 When comparing the systemic glucagon receptor-deficient mice at 4 weeks of age (Fig 3B) with

368 those at 10 weeks of age (Fig 2C), we observed a significant increase in PP-cell mass at 10 weeks

369 of age. Corresponding to this substantial change, the number of GCG^+ PP^+ double-positive cells

370 in 4 week-old glucagon receptor-deficient mice was comparable to that in wild-type mice (Fig

371 3D). However, in 10 week-old glucagon receptor-deficient mice, the number of GCG^+ PP^+

372 double-positive cells robustly increased compared with that in both wild-type mice and 4 week-

373 old glucagon receptor-deficient mice (Fig 3D). We propose that this increase in GCG^+ PP^+ double-

374 positive cells accounts for the substantial increase in PP-cell mass observed in 10 week-old

375 glucagon receptor-deficient mice.

376 Owing to glucagon dysfunction in the liver, the hyperplasia of PP cells and the emergence

377 of multi-hormone-producing cells were observed (Fig 4), associated with an increase in blood

378 amino acid levels. Similar to α-cell hyperplasia, the increased amino acids levels may have

379 triggered these phenomena [18, 20, 21]. Supporting this hypothesis, culturing isolated islets in a

380 high-glutamine medium resulted in an increased number of PP cells (Fig 5C) and an increase in

381 GCG^+ PP^+ double-positive cells (Fig 5D). Furthermore, we compared PP-cell mass in 10 week-

old systemic glucagon receptor-deficient mice (Fig 2D) and liver-specific glucagon receptor-deficient mice (Fig 4C). Despite being the same age, there was a significant difference in the PP-cell mass between the two groups. A potential explanation for this difference is the variation in plasma amino acid levels between the two groups. As shown in S3 Fig, plasma amino acid levels in systemic glucagon receptor-deficient mice were higher than those in liver-specific glucagon receptor-deficient mice. Particularly in terms of glutamine levels, systemic glucagon receptor-deficient mice demonstrated significantly higher values (S4 Fig). We believe that this difference in amino acid levels accounts for the variation in PP-cell mass of these mice at the same age.

Our results demonstrate that increased blood amino acid levels resulting from impaired glucagon action in the liver activates the mTOR pathway in α cells, leading to the emergence of GCG^+ PP^+ double-positive cells. Previous studies have shown that forced expression of Aristaless-related homeobox (ARX) protein, a key transcription factor that determines the fate of α cells [39-41], in the embryonic pancreas or developing islet cells leads to a marked increase in α cells, accompanied by the loss of β and δ cell. Interestingly, under these conditions, the number of PP cells also increases substantially [39]. In humans with ARX mutations, β, δ, and ghrelin-secreting ε cells are present normally, whereas α and PP cells are deficient [42]. During

398 development, α and PP cells differentiate from a common α/PP precursor [40, 43, 44]. This
399 suggests that their differentiation may also depend on transcription factors other than ARX.
400 However, the mechanisms that distinguish these two cell types and maintain their respective
401 identities remain unclear. Since some transcription factors, such as ARX, are commonly active in
402 both cell types, it is believed that under normal conditions, PP protein expression is suppressed in
403 α cells to preserve their identity. Collectively, our findings suggest that suppression of the mTOR
404 pathway in α cells inhibits the expression of factors, including PP proteins, that drive PP-cell
405 characteristics. Future studies should focus on elucidating how the mTOR pathway regulates these
406 factors in α cells. Furthermore, we demonstrated that glucagon dysfunction leads to the emergence
407 of multi-hormone-producing cells, including PP^+ INS^+ double-positive cells (Fig 4E) and PP^+
408 GFP^+ SST^+ triple-positive cells (Fig 1B). However, the precise mechanistic link between glucagon
409 dysfunction and the appearance of these cells remains unclear. Interestingly, a subset of pituitary
410 cells is known to produce multiple hormones and function under specific physiological conditions
411 such as growth, stress response, and reproduction. Gene expression analysis further suggests that
412 these multihormone cells originate from undifferentiated or plastic cells [26]. Given these
413 findings, one hypothesis is that the increase in blood amino acid levels due to impaired glucagon

414 action in the liver activates the mTOR pathway in α cells, leading to enhanced cell proliferation

415 and increased cellular plasticity. Consequently, α cells may shift to a more undifferentiated state,

416 resulting in an increased emergence of multi-hormone-producing cells, including GCG^+ PP^+

417 double-positive cells. Future studies are needed to elucidate how these multi-hormone-producing

418 cells influence the progression and regulation of pathological conditions caused by glucagon

419 dysfunction.

420 In conclusion, impaired glucagon signaling activates the mTOR pathway via

421 hyperaminoacidemia, particularly elevated glutamine levels, inducing not only α-cell hyperplasia

422 but also PP-cell hyperplasia and the formation of multi-hormone-producing cells. Inhibition of

423 mTOR suppresses these changes. This study reveals a novel mechanism by which glucagon

424 dysfunction alters pancreatic endocrine cell composition, highlighting the critical role of mTOR

425 in endocrine cell plasticity.

426

427 **Conflicts of interest**

428 The authors declare that they have no conflicts of interest associated with this study.

429

430 **Acknowledgments**

431 This work was supported by Grants-in-Aid for Scientific Research (18K08501 and
432 21K08547 to YN) from the Ministry of Education, Culture, Sports, Science, and Technology,
433 Japan. We extend our heartfelt gratitude to W. Mizutani, Y. Tamura, A. Suda, N. Kagami, K. Iizuka,
434 A. Fukaishi, Y. Miyazaki, H. Netsu, and T. Ishizaka of the Fujitani Laboratory (Gunma University,
435 Gunma, Japan) for their invaluable technical assistance. We are also deeply grateful to Dr. H.A.
436 Popiel (Tokyo Medical University, Tokyo, Japan) for critically reviewing the manuscript. Our
437 sincere thanks go to the members of Dr. Y. Kitamura's laboratory and Dr. J. Shirakawa's
438 laboratory (both from IMCR, Gunma University) for their insightful discussions. We also thank
439 Dr. A. Oue, Dr. T. Kakinuma, and other members of the Bioresource Center at Gunma University
440 for their generous support of general research on mice.

441

Author contributions

Conceptualization: Yuko Nakagawa, Ayako Fukunaka, Takashi Sato, Yoshio Fujitani

Data curation: Yuko Nakagawa

Funding acquisition: Yuko Nakagawa, Yoshio Fujitani

Investigation: Yuko Nakagawa, Takuro Horii, Takashi Nishimura

Methodology: Yuko Nakagawa, Yoshio Fujitani

Project administration: Yoshio Fujitani

Resources: Takuro Horii, Izuho Hatada, Masaki Kobayashi, Tadahiro Kitamura, Yoshitaka Hayashi

Supervision: Yoshio Fujitani

Validation: Yuko Nakagawa

Visualization: Yuko Nakagawa

Writing – original draft: Yuko Nakagawa, Yoshio Fujitani

Writing – review & editing: Yuko Nakagawa, Yoshio Fujitani

457 **References**

458 **1.** Hayashi Y, Seino Y. Regulation of amino acid metabolism and alpha-cell proliferation

459 by glucagon. J Diabetes Investig. 2018; 9(3): 464-472.

460 https://doi.org/10.1111/jdi.12797. PMID: 29314731.

461 **2.** Takeuchi Y, Yahagi N, Aita Y, Mehrazad-Saber Z, Ho MH, Huyan Y, et al. FoxO-KLF15

462 pathway switches the flow of macronutrients under the control of insulin. iScience.

463 2021; 24(12): 103446. https://doi.org/10.1016/j.isci.2021.103446. PMID: 34988390.

464 **3.** Salinno C, Cota P, Bastidas-Ponce A, Tarquis-Medina M, Lickert H, Bakhti M. beta-

465 Cell Maturation and Identity in Health and Disease. Int J Mol Sci. 2019; 20(21).

466 https://doi.org/10.3390/ijms20215417. PMID: 31671683.

467 **4.** Almaca J, Caicedo A, Landsman L. Beta cell dysfunction in diabetes: the islet

468 microenvironment as an unusual suspect. Diabetologia. 2020; 63(10): 2076-2085.

469 https://doi.org/10.1007/s00125-020-05186-5. PMID: 32894318.

470 **5.** Philips S, Shah SN, Vikram R, Verma S, Shanbhogue AK, Prasad SR. Pancreatic

471 endocrine neoplasms: a current update on genetics and imaging. Br J Radiol. 2012;

472 85(1014): 682-696. https://doi.org/10.1259/bjr/85014761. PMID: 22253347.

473 **6.** Wang Y, Ni Q, Sun J, Xu M, Xie J, Zhang J, et al. Paraneoplastic beta Cell
474 Dedifferentiation in Nondiabetic Patients with Pancreatic Cancer. J Clin Endocrinol
475 Metab. 2020; 105(4). https://doi.org/10.1210/clinem/dgz224. PMID: 31781763.
476 **7.** Dean ED. A Primary Role for alpha-Cells as Amino Acid Sensors. Diabetes. 2020;
477 69(4): 542-549. https://doi.org/10.2337/dbi19-0021. PMID: 31653720.
478 **8.** Hayashi Y, Yamamoto M, Mizoguchi H, Watanabe C, Ito R, Yamamoto S, et al. Mice
479 deficient for glucagon gene-derived peptides display normoglycemia and hyperplasia of
480 islet alpha-cells but not of intestinal L-cells. Mol Endocrinol. 2009; 23(12): 1990-1999.
481 https://doi.org/10.1210/me.2009-0296. PMID: 19819987.
482 **9.** Takagi Y, Kinoshita K, Ozaki N, Seino Y, Murata Y, Oshida Y, et al. Mice Deficient in
483 Proglucagon-Derived Peptides Exhibit Glucose Intolerance on a High-Fat Diet but Are
484 Resistant to Obesity. PLoS One. 2015; 10(9): e0138322.
485 https://doi.org/10.1371/journal.pone.0138322. PMID: 26378455.
486 **10.** Gelling RW, Du XQ, Dichmann DS, Romer J, Huang H, Cui L, et al. Lower blood
487 glucose, hyperglucagonemia, and pancreatic alpha cell hyperplasia in glucagon receptor
488 knockout mice. Proc Natl Acad Sci U S A. 2003; 100(3): 1438-1443.

https://doi.org/10.1073/pnas.0237106100. PMID: 12552113.

11. Sorensen H, Winzell MS, Brand CL, Fosgerau K, Gelling RW, Nishimura E, et al. Glucagon receptor knockout mice display increased insulin sensitivity and impaired beta-cell function. Diabetes. 2006; 55(12): 3463-3469. https://doi.org/10.2337/db06-0307. PMID: 17130493.

12. Vuguin PM, Kedees MH, Cui L, Guz Y, Gelling RW, Nejathaim M, et al. Ablation of the glucagon receptor gene increases fetal lethality and produces alterations in islet development and maturation. Endocrinology. 2006; 147(9): 3995-4006. https://doi.org/10.1210/en.2005-1410. PMID: 16627579.

13. Longuet C, Robledo AM, Dean ED, Dai C, Ali S, McGuinness I, et al. Liver-specific disruption of the murine glucagon receptor produces alpha-cell hyperplasia: evidence for a circulating alpha-cell growth factor. Diabetes. 2013; 62(4): 1196-1205. https://doi.org/10.2337/db11-1605. PMID: 23160527.

14. Yu R. Pancreatic alpha-cell hyperplasia: facts and myths. J Clin Endocrinol Metab. 2014; 99(3): 748-756. https://doi.org/10.1210/jc.2013-2952. PMID: 24285676.

15. Yu R, Zheng Y, Lucas MB, Tong YG. Elusive liver factor that causes pancreatic alpha

505 cell hyperplasia: A review of literature. World J Gastrointest Pathophysiol. 2015; 6(4):
506 131-139. https://doi.org/10.4291/wjgp.v6.i4.131. PMID: 26600971.
507 **16.** Cidade-Rodrigues C, Santos AP, Calheiros R, Santos S, Matos C, Moreira AP, et al.
508 Non-functional alpha-cell hyperplasia with glucagon-producing NET: a case report.
509 Front Endocrinol (Lausanne). 2024; 15: 1405835.
510 https://doi.org/10.3389/fendo.2024.1405835. PMID: 39309109.
511 **17.** Okamoto H, Kim J, Aglione J, Lee J, Cavino K, Na E, et al. Glucagon Receptor
512 Blockade With a Human Antibody Normalizes Blood Glucose in Diabetic Mice and
513 Monkeys. Endocrinology. 2015; 156(8): 2781-2794. https://doi.org/10.1210/en.2015-
514 1011. PMID: 26020795.
515 **18.** Solloway MJ, Madjidi A, Gu C, Eastham-Anderson J, Clarke HJ, Kljavin N, et al.
516 Glucagon Couples Hepatic Amino Acid Catabolism to mTOR-Dependent Regulation of
517 alpha-Cell Mass. Cell Rep. 2015; 12(3): 495-510.
518 https://doi.org/10.1016/j.celrep.2015.06.034. PMID: 26166562.
519 **19.** Bozadjieva N, Blandino-Rosano M, Chase J, Dai XQ, Cummings K, Gimeno J, et al.
520 Loss of mTORC1 signaling alters pancreatic alpha cell mass and impairs glucagon

521 secretion. J Clin Invest. 2017; 127(12): 4379-4393. https://doi.org/10.1172/JCI90004.

522 PMID: 29106387.

523 **20.** Dean ED, Li M, Prasad N, Wisniewski SN, Von Deylen A, Spaeth J, et al. Interrupted

524 Glucagon Signaling Reveals Hepatic alpha Cell Axis and Role for L-Glutamine in alpha

525 Cell Proliferation. Cell Metab. 2017; 25(6): 1362-1373 e1365.

526 https://doi.org/10.1016/j.cmet.2017.05.011. PMID: 28591638.

527 **21.** Kim J, Okamoto H, Huang Z, Anguiano G, Chen S, Liu Q, et al. Amino Acid

528 Transporter Slc38a5 Controls Glucagon Receptor Inhibition-Induced Pancreatic alpha

529 Cell Hyperplasia in Mice. Cell Metab. 2017; 25(6): 1348-1361 e1348.

530 https://doi.org/10.1016/j.cmet.2017.05.006. PMID: 28591637.

531 **22.** Song Y, Koehler JA, Baggio LL, Powers AC, Sandoval DA, Drucker DJ. Gut-

532 Proglucagon-Derived Peptides Are Essential for Regulating Glucose Homeostasis in

533 Mice. Cell Metab. 2019; 30(5): 976-986 e973.

534 https://doi.org/10.1016/j.cmet.2019.08.009. PMID: 31495689.

535 **23.** Smith DK, Kates L, Durinck S, Patel N, Stawiski EW, Kljavin N, et al. Elevated Serum

536 Amino Acids Induce a Subpopulation of Alpha Cells to Initiate Pancreatic

537 Neuroendocrine Tumor Formation. Cell Rep Med. 2020; 1(5): 100058.
538 https://doi.org/10.1016/j.xcrm.2020.100058. PMID: 33205067.
539 **24.** Fukaishi T, Nakagawa Y, Fukunaka A, Sato T, Hara A, Nakao K, et al. Characterisation
540 of Ppy-lineage cells clarifies the functional heterogeneity of pancreatic beta cells in
541 mice. Diabetologia. 2021; 64(12): 2803-2816. https://doi.org/10.1007/s00125-021-
542 05560-x. PMID: 34498099.
543 **25.** Ramond C, Beydag-Tasoz BS, Azad A, van de Bunt M, Petersen MBK, Beer NL, et al.
544 Understanding human fetal pancreas development using subpopulation sorting, RNA
545 sequencing and single-cell profiling. Development. 2018; 145(16).
546 https://doi.org/10.1242/dev.165480. PMID: 30042179.
547 **26.** Fontaine R, Rahmad Royan M, Henkel C, Hodne K, Ager-Wick E, Weltzien FA.
548 Pituitary multi-hormone cells in mammals and fish: history, origin, and roles. Front
549 Neuroendocrinol. 2022; 67: 101018. https://doi.org/10.1016/j.yfrne.2022.101018.
550 PMID: 35870647.
551 **27.** Perez-Frances M, van Gurp L, Abate MV, Cigliola V, Furuyama K, Bru-Tari E, et al.
552 Pancreatic Ppy-expressing gamma-cells display mixed phenotypic traits and the

553 adaptive plasticity to engage insulin production. Nat Commun. 2021; 12(1): 4458.
554 https://doi.org/10.1038/s41467-021-24788-0. PMID: 34294685.
555 **28.** Horii T, Kobayashi R, Hatada I. Generation of Floxed Mice by Sequential
556 Electroporation. Methods Mol Biol. 2023; 2637: 135-147. https://doi.org/10.1007/978-
557 1-0716-3016-7_11. PMID: 36773144.
558 **29.** Sakai K, Miyazaki J. A transgenic mouse line that retains Cre recombinase activity in
559 mature oocytes irrespective of the cre transgene transmission. Biochem Biophys Res
560 Commun. 1997; 237(2): 318-324. https://doi.org/10.1006/bbrc.1997.7111. PMID:
561 9268708.
562 **30.** Sato T, Mushiake S, Kato Y, Sato K, Sato M, Takeda N, et al. The Rab8 GTPase
563 regulates apical protein localization in intestinal cells. Nature. 2007; 448(7151): 366-
564 369. https://doi.org/10.1038/nature05929. PMID: 17597763.
565 **31.** Postic C, Magnuson MA. DNA excision in liver by an albumin-Cre transgene occurs
566 progressively with age. Genesis. 2000; 26(2): 149-150.
567 https://doi.org/10.1002/(sici)1526-968x(200002)26:2<149::aid-gene16>3.0.co;2-v.
568 PMID: 10686614.

569 **32.** Hara A, Nakagawa Y, Nakao K, Tamaki M, Ikemoto T, Shimada M, et al. Development
570 of monoclonal mouse antibodies that specifically recognize pancreatic polypeptide.
571 Endocr J. 2019; 66(5): 459-468. https://doi.org/10.1507/endocrj.EJ18-0441. PMID:
572 30842364.
573 **33.** Takahashi M, Miyatsuka T, Suzuki L, Osonoi S, Himuro M, Miura M, et al. Biphasic
574 changes in beta-cell mass around parturition are accompanied by increased serotonin
575 production. Sci Rep. 2020; 10(1): 4962. https://doi.org/10.1038/s41598-020-61850-1.
576 PMID: 32188885.
577 **34.** Saito D, Nakagawa Y, Sato T, Fukunaka A, Pereye OB, Maruyama N, et al.
578 Establishment of an enzyme-linked immunosorbent assay for mouse pancreatic
579 polypeptide clarifies the regulatory mechanism of its secretion from pancreatic gamma
580 cells. PLoS One. 2022; 17(8): e0269958. https://doi.org/10.1371/journal.pone.0269958.
581 PMID: 35976945.
582 **35.** Nishimura T. Feedforward Regulation of Glucose Metabolism by Steroid Hormones
583 Drives a Developmental Transition in Drosophila. Curr Biol. 2020; 30(18): 3624-3632
584 e3625. https://doi.org/10.1016/j.cub.2020.06.043. PMID: 32679096.

585 **36.** Yamada T, Hironaka KI, Habara O, Morishita Y, Nishimura T. A developmental
586 checkpoint directs metabolic remodelling as a strategy against starvation in Drosophila.
587 Nat Metab. 2020; 2(10): 1096-1112. https://doi.org/10.1038/s42255-020-00293-4.
588 PMID: 33046910.
589 **37.** Charron MJ, Vuguin PM. Lack of glucagon receptor signaling and its implications
590 beyond glucose homeostasis. J Endocrinol. 2015; 224(3): R123-130.
591 https://doi.org/10.1530/JOE-14-0614. PMID: 25568163.
592 **38.** Gu L, Cui X, Lang S, Wang H, Hong T, Wei R. Glucagon receptor antagonism increases
593 mouse pancreatic delta-cell mass through cell proliferation and duct-derived neogenesis.
594 Biochem Biophys Res Commun. 2019; 512(4): 864-870.
595 https://doi.org/10.1016/j.bbrc.2019.03.148. PMID: 30929915.
596 **39.** Collombat P, Hecksher-Sorensen J, Krull J, Berger J, Riedel D, Herrera PL, et al.
597 Embryonic endocrine pancreas and mature beta cells acquire alpha and PP cell
598 phenotypes upon Arx misexpression. J Clin Invest. 2007; 117(4): 961-970.
599 https://doi.org/10.1172/JCI29115. PMID: 17404619.
600 **40.** Bramswig NC, Kaestner KH. Transcriptional regulation of alpha-cell differentiation.

601 Diabetes Obes Metab. 2011; 13 Suppl 1: 13-20. https://doi.org/10.1111/j.1463-
602 1326.2011.01440.x. PMID: 21824252.
603 **41.** Wilcox CL, Terry NA, Walp ER, Lee RA, May CL. Pancreatic alpha-cell specific
604 deletion of mouse Arx leads to alpha-cell identity loss. PLoS One. 2013; 8(6): e66214.
605 https://doi.org/10.1371/journal.pone.0066214. PMID: 23785486.
606 **42.** Gage BK, Asadi A, Baker RK, Webber TD, Wang R, Itoh M, et al. The Role of ARX in
607 Human Pancreatic Endocrine Specification. PLoS One. 2015; 10(12): e0144100.
608 https://doi.org/10.1371/journal.pone.0144100. PMID: 26633894.
609 **43.** Khadra A, Schnell S. Development, growth and maintenance of beta-cell mass: models
610 are also part of the story. Mol Aspects Med. 2015; 42: 78-90.
611 https://doi.org/10.1016/j.mam.2015.01.005. PMID: 25720614.
612 **44.** Zhong F, Jiang Y. Endogenous Pancreatic beta Cell Regeneration: A Potential Strategy
613 for the Recovery of beta Cell Deficiency in Diabetes. Front Endocrinol (Lausanne).
614 2019; 10: 101. https://doi.org/10.3389/fendo.2019.00101. PMID: 30842756.
615

616 **Figure legends**

617 **Fig. 1. Deficiency of proteins encoded by the proglucagon gene induces PP-cell hyperplasia**

618 **and the formation of multi-hormone-producing cells**

619 (A) Representative immunofluorescence staining of GCG or GFP (green), PP (red), and nuclei

620 (DAPI; blue) in pancreas sections from 40 week old $GCG^{+/+}$ mice and $Gcg^{gfp/gfp}$ mice. A magnified

621 view of the boxed region is shown on the very right. (B) Representative immunofluorescence

622 staining of PP (blue), GCG or GFP (green), and SST (red) in pancreas sections from 40 week-old

623 $Gcg^{+/+}$ mice and $Gcg^{gfp/gfp}$ mice (B). Scale bars represent 30 μm or 50 μm.

624

625 **Fig 2. Glucagon signaling deficiency induces PP-cell hyperplasia and the appearance of**

626 **GCG^+ PP^+ double-positive cells**

627 (A) Schematic diagram of the loxP target site. (B) Representative immunofluorescence staining

628 of GCG (green), PP (red), and nuclei (DAPI; blue) in pancreas sections from 10 week-old $Gcgr^{+/+}$

629 mice and $Gcgr^{\Delta/\Delta}$ mice. Magnified images of the boxed region are shown at the bottom. Scale bar

630 represents 30 μm. PP-cell mass (C) and the proportion of GCG^+ PP^+ cells among the GCG^+ cells

631 (D) in 10 week-old $Gcgr^{+/+}$ mice and $Gcgr^{\Delta/\Delta}$ mice (n = 4–7 mice). Data are shown as the mean

632 ± SEM, and analyzed by the two-tailed unpaired Student *t*-test. $^{**}p < 0.01$, $^{***}p < 0.001$.

633

634 **Fig 3. PP-cell hyperplasia involves both the self-proliferation of PP cells and an increase in**

635 **GCG^{+} PP^{+} double-positive cells**

636 (A) Representative immunofluorescence staining of GCG (green), PP (red), and nuclei (DAPI;

637 blue) in pancreas sections from 4 week-old *Gcgr*$^{+/+}$ mice and *Gcgr*$^{\Delta/\Delta}$ mice. Scale bar represents

638 30 μm. (B) PP-cell mass in 4week-old *Gcgr*$^{+/+}$ mice and *Gcgr*$^{\Delta/\Delta}$ mice (n = 6 mice each). (C)

639 Representative immunofluorescence staining of GCG (green), PP (red), and nuclei (DAPI; blue)

640 in pancreas sections from 4 week-old and 10 week-old *Gcgr*$^{+/+}$ mice and *Gcgr*$^{\Delta/\Delta}$ mice. Scale bar

641 represents 30 μm. (D) Proportions of GCG^{+} PP^{+} cells among GCG^{+} cells in 4 week-old and 10

642 week-old *Gcgr*$^{+/+}$ mice and *Gcgr*$^{\Delta/\Delta}$ mice (n = 4 mice each). (E) Representative

643 immunofluorescence staining of PP (blue), GCG (green), and Ki67 (red) in pancreas sections from

644 4 week-old *Gcgr*$^{+/+}$ mice and *Gcgr*$^{\Delta/\Delta}$ mice. Scale bar represents 30 μm. A magnified image of the

645 boxed region is shown on the very right. (F) Proportions of Ki67^{+} PP^{+} GCG^{-} cells among PP^{+}

646 cells in 10 week-old *Gcgr*$^{+/+}$ mice and *Gcgr*$^{\Delta/\Delta}$ mice (n = 4 mice each). Data are shown as the

647 mean ± SEM, and analyzed by the two-tailed unpaired Student *t*-test (B and F) or one-way

648 ANOVA followed by the Tukey test (D). $^{**}p < 0.01$, $^{***}p < 0.001$, $^{****}p < 0.0001$.

649

650 **Fig 4. Glucagon dysfunction in the liver induces PP-cell hyperplasia and the appearance of**

651 **GCG^{+} PP^{+} double-positive cells**

652 (A) Representative immunofluorescence staining of GCG (green), PP (red), and nuclei (DAPI;

653 blue) in pancreas sections from 10 week-old *Gcgr*$^{f/f}$ mice and Alb-*Cre;Gcgr*$^{f/f}$ mice. Scale bar

654 represents 30 μm. The PP-cell mass (B) and the proportion of GCG^{+} PP^{+} cells among GCG^{+} cells

655 (C) in 10 week-old *Gcgr*$^{f/f}$ mice and Alb-*Cre;Gcgr*$^{f/f}$ mice (n = 5 mice each) are shown. (D)

656 Representative immunofluorescence staining of GCG (green), PP (red), and nuclei (DAPI; blue)

657 in pancreas sections from 40 week-old *Gcgr*$^{f/f}$ mice and Alb-*Cre;Gcgr*$^{f/f}$ mice. (E) Representative

658 immunofluorescence staining of INS (green), PP (red), and nuclei (blue) in pancreas sections from

659 40 week-old *Gcgr*$^{f/f}$ mice and Alb-*Cre;Gcgr*$^{f/f}$ mice. Scale bar represents 30 μm. In (B) and (C),

660 data are shown as the mean ± SEM, and analyzed by the two-tailed unpaired Student *t*-test. $^{*}p <$

661 0.05, $^{**}p < 0.01$. In C, D, and E, magnified images of the boxed regions are shown in the bottom

662 row.

663

664 **Fig 5. GCG^+ PP^+ double-positive cells are increased in isolated islets upon incubation in high**

665 **concentrations of glutamine, and this increase is mediated by the mTOR pathway**

666 (A) Representative immunofluorescence staining of PP (red), GCG (white), and nuclei (blue) in

667 pancreas islets from 10 week-old wild-type mice, untreated (Ctrl, upper panels) or incubated with

668 a high concentration glutamine (Gln, lower panels). Scale bar represents 30 μm. Magnified

669 images of the boxed region are shown at the bottom. The proportion of GCG^+ cells among islet

670 cells (B) (n = 10 islets), the proportion of PP cells among islet cells (C) (n = 10 islets), and the

671 proportion of GCG^+ PP^+ cells among GCG^+ islet cells (D) (n = 10 islets) from 10 week-old wild-

672 type mice, either untreated (Ctrl) or incubated in a high concentration of glutamine (Gln). (E)

673 Representative immunofluorescence staining of PP (red) and GCG (white) in pancreatic islets

674 isolated from 10 week-old wild-type mice. Untreated islets (Ctrl, left panel), islets incubated with

675 a high concentration of glutamine (Gln, middle panel), and islets incubated with both a high

676 concentration of glutamine and rapamycin (Gln+Rap, right panel) are shown. Scale bar represents

677 30 μm. (F) Proportions of GCG^+ PP^+ cells among GCG^+ cells of the islets (n = 10 islets) from 10

678 week-old wild-type mice, which were untreated (Ctrl), incubated with a high concentration of

679 glutamine (Gln), or incubated with both a high concentration of glutamine and rapamycin

680 (Gln+Rap). Data are shown as the mean ± SEM, and analyzed by the two-tailed unpaired Student

681 *t*-test (B–D) or one-way ANOVA followed by the Tukey test (F). $^{**}p < 0.01$, $^{***}p < 0.001$, ns,

682 not significant.

683

684 **Supporting information**

685 **S1 Fig. α-cell mass in 10 week-old *Gcgr*$^{f/f}$ mice and Alb-*Cre*:*Gcgr*$^{f/f}$ mice**

686 Data are shown as the mean ± SEM, and analyzed by the two-tailed unpaired Student *t*-test. $^{*}p <$

687 0.05; n = 4 each.

688

689 **S2 Fig. PP-cell mass in in 40 week-old *Gcgr*$^{f/f}$ mice and Alb-*Cre*:*Gcgr*$^{f/f}$ mice**

690 Data are shown as the mean ± SEM, and analyzed by the two-tailed unpaired Student *t*-test. $^{*}p <$

691 0.05. n = 6 each.

692

693 **S3 Fig. Plasma levels of individual amino acids in 10 week-old *Gcgr*$^{f/f}$, Alb-*Cre*:*Gcgr*$^{f/f}$,**

694 ***Gcgr*$^{+/+}$, and *Gcgr*$^{\Delta/\Delta}$ mice**

695 Data are shown as the mean ± SEM (n = 4–7 mice each).

696

697 **S4 Fig. Plasma glutamine levels in 10 week-old *Gcgr*$^{f/f}$, Alb-*Cre*:*Gcgr*$^{f/f}$, *Gcgr*$^{+/+}$, and *Gcgr*$^{\Delta/\Delta}$**

698 **mice**

699 Data are shown as the mean ± SEM, and analyzed by one-way ANOVA followed by the Tukey

700 test. *$p < 0.05$, **$p < 0.01$, ****$p < 0.0001$; ns, not significant.

701

702 **S5 Fig. Activation of the mTOR pathway in GCG^{+} PP^{+} cells from 40 week-old *Gcgr*$^{+/+}$ mice**

703 **and *Gcgr*$^{\Delta/\Delta}$ mice**

704 Representative immunofluorescence staining of GCG (green), pS6 (red), and PP (white) from 40

705 week-old *Gcgr*$^{+/+}$ mice and *Gcgr*$^{\Delta/\Delta}$ mice. Scale bar represents 30 μm. Enlarged images of the

706 boxed region are shown on the very right.

707

708 **S6 Fig. Comparison of the number of PP^{+} positive-cells based on the presence or absence of**

709 **glucagon and pS6 signals in 4 week-old *Gcgr*$^{+/+}$ mice and *Gcgr*$^{\Delta/\Delta}$ mice**

710 (A) Representative immunofluorescence staining of GCG (green), pS6 (red), and PP (white) from

711 4 week-old *Gcgr*$^{+/+}$ mice and *Gcgr*$^{\Delta/\Delta}$ mice. Scale bar represents 30 μm. Enlarged images of the

712 boxed region are shown on the very right. (B) Changes in the number of PP^{+} positive cells based

713 on the presence or absence of glucagon and pS6 signals in 4 week-old *Gcgr*$^{+/+}$ mice and *Gcgr*$^{\Delta/\Delta}$

714 micen (n = 25 islets). Data are shown as the mean ± SEM, and analyzed by one-way ANOVA

715 followed by the Tukey test. $^{**}p < 0.01$, $^{***}p < 0.001$, $^{****}p < 0.0001$; ns, not significant.

716

Locus	Target	ssODN
Left loxP	GcgrL4 (5′- ATGGCAAGATCACTGGCCAG -3′)	GcgrL4loxP (5′- AAATGTTGCTGGGCTGGAGAGGGAGGTAGTCATGGCA TCTAGATGGCAAGATCACTGGCCAATATTATAACTTCGT ATAATGTATGCTATACGAAGTTATAGGGGATGCCCCTTG TGGCCCATATCAGGGAGGCAGCCCCTTTAGATGCAGG CTCCGTGT -3′)
Right loxP	GcgrR6 (5′- GAATTCCCTGAGGACCTAGG -3′)	GcgrR6loxP (5′- GGCCATTTGTCACCAGGAAAGGCAAGGACCACCTCATA CACTGAATTCCCTGAGGACCTAATAACTTCGTATAGCAT ACATTATACGAAGTTATCTCGAGGGGGGACCTGACATC CAACACATGCAACCTTAATAATGGGGATGGAGATATGGT CATACC -3′)

Table 1. Sequences of target crRNAs flanking exons 4 to 13 of the *Gcgr* gene, and corresponding donor single-stranded oligodeoxynucleotides (ssODNs), including loxP

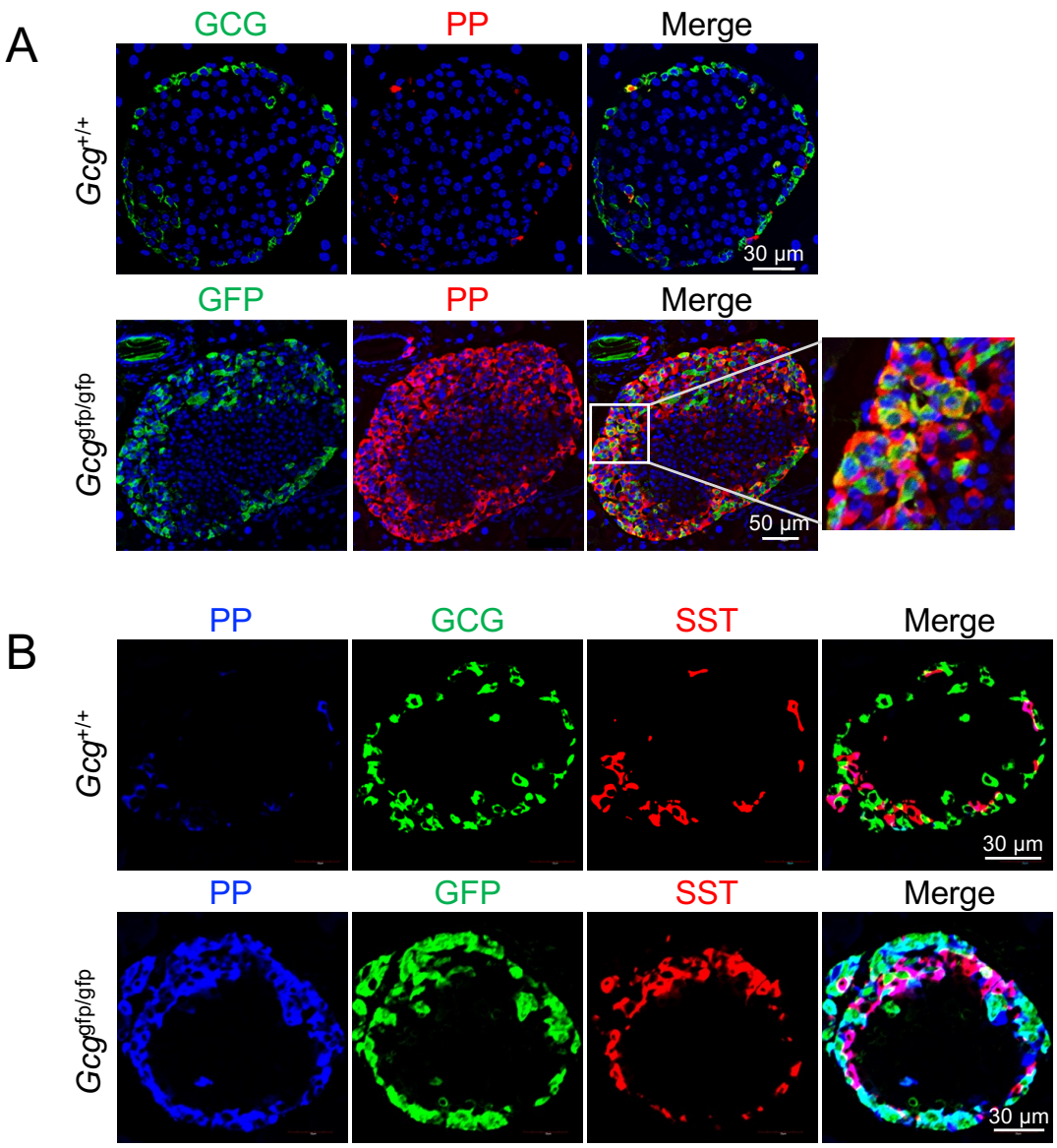

Fig. 1. Deficiency of proteins encoded by the proglucagon gene induces PP-cell hyperplasia and the formation of multi-hormone-producing cells

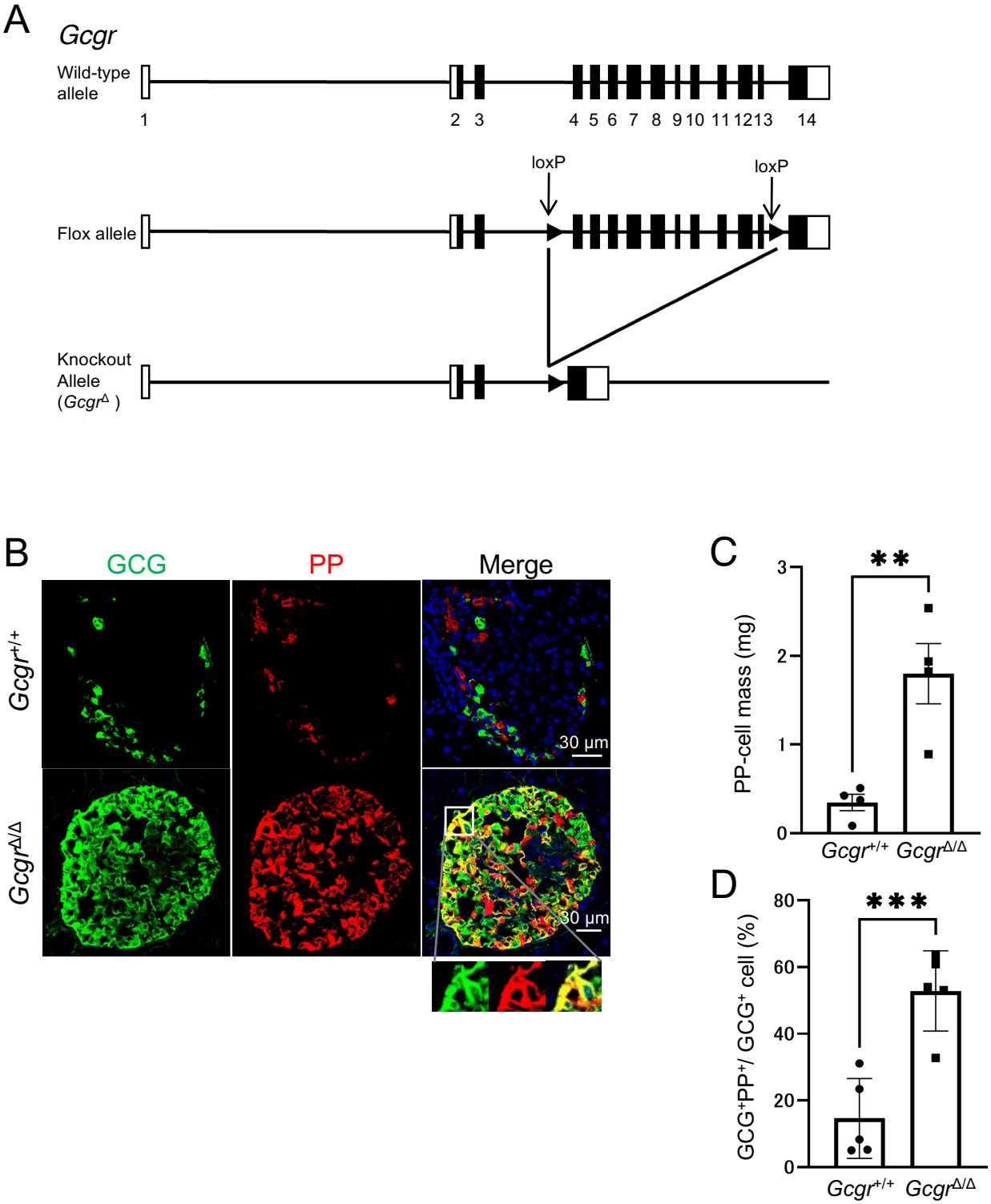

Fig 2. Glucagon signaling deficiency induces PP-cell hyperplasia and the appearance of GCG^{+} PP^{+} double-positive cells

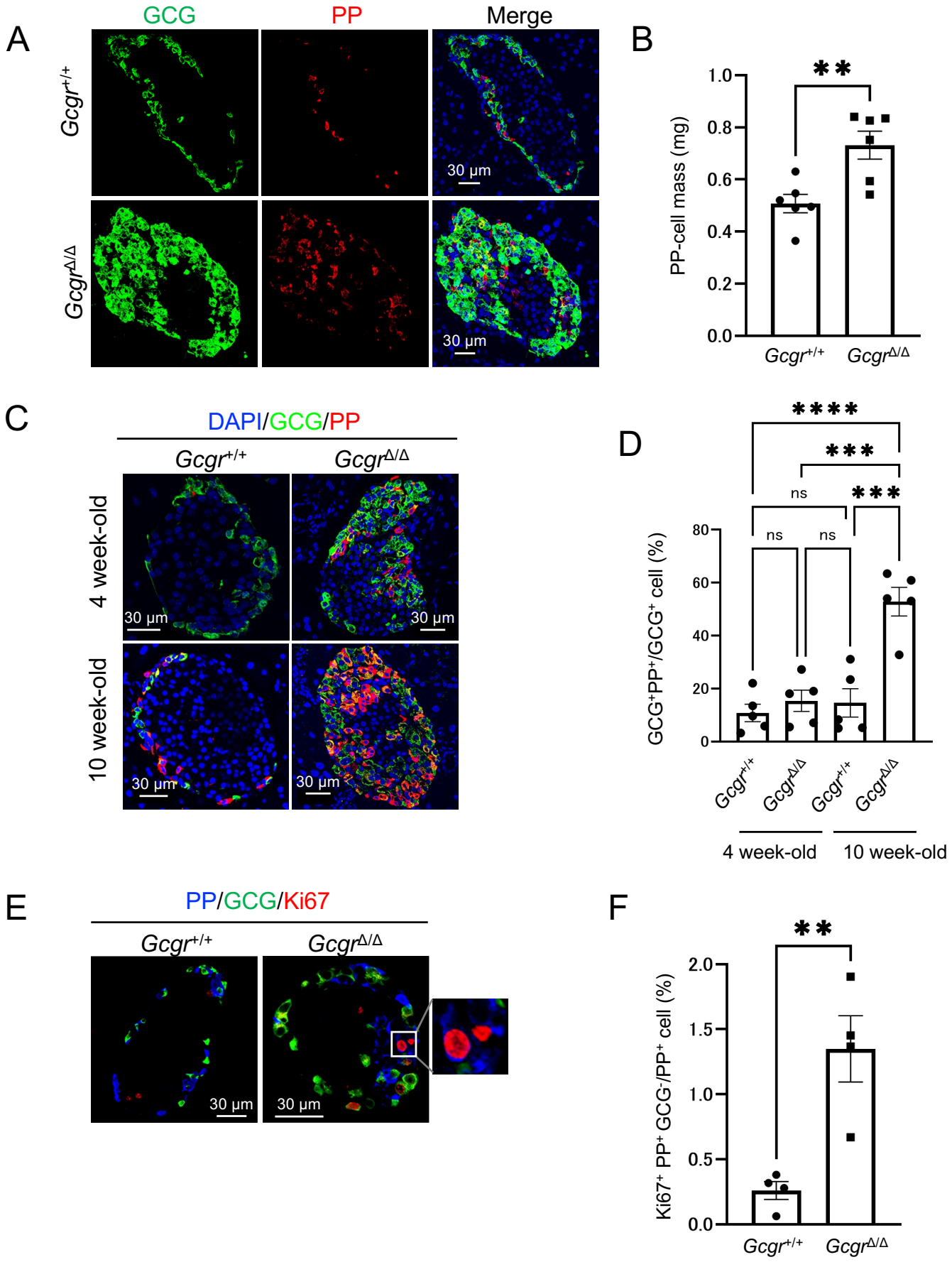

Fig 3. PP-cell hyperplasia involves both the self-proliferation of PP cells and an increase in GCG$^+$ PP$^+$ double-positive cells

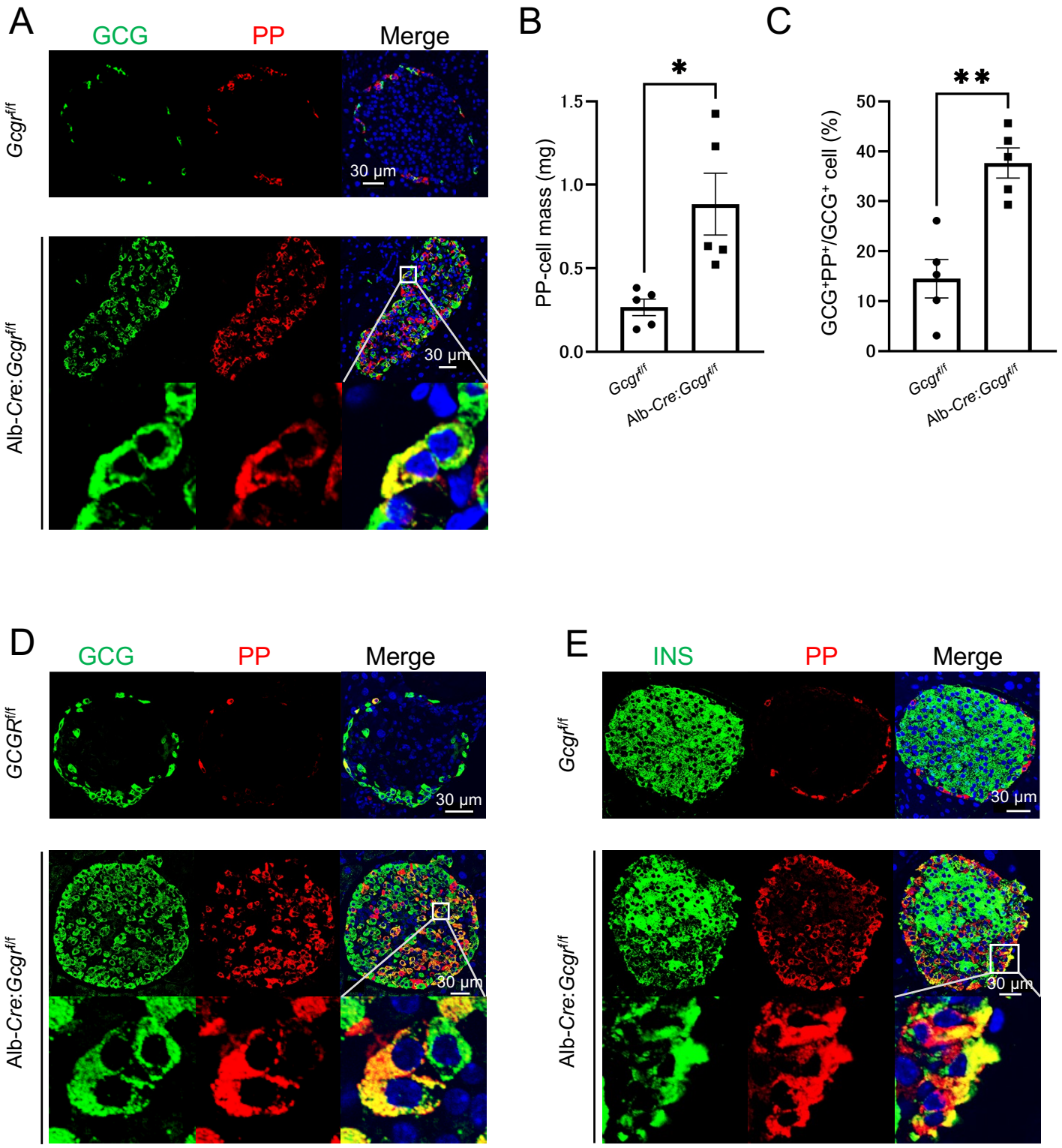

Fig 4. Glucagon dysfunction in the liver induces PP-cell hyperplasia and the appearance of GCG$^+$ PP$^+$ double-positive cells

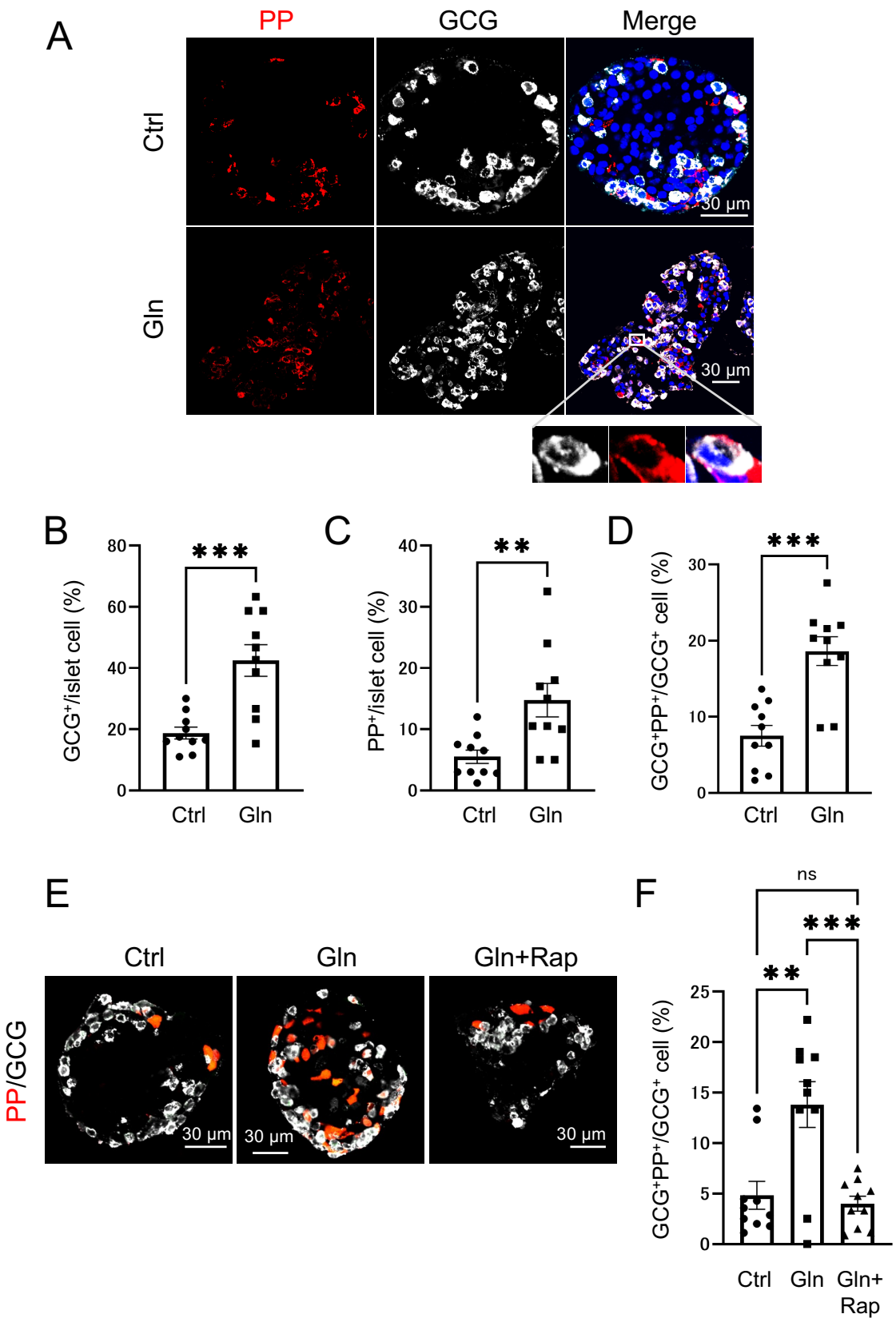

Fig 5. GCG+ PP+ double-positive cells are increased in isolated islets upon incubation in high concentrations of glutamine, and this increase is mediated by the mTOR pathway

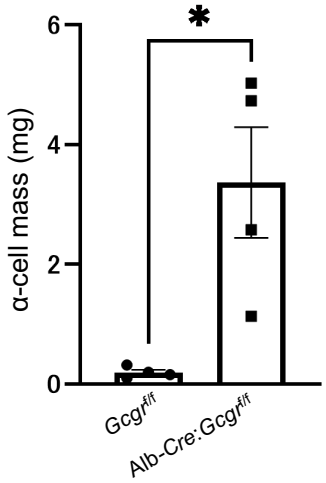

S1 Fig. α-cell mass in 10 week-old *Gcgr*$^{f/f}$ mice and Alb-*Cre*:*Gcgr*$^{f/f}$ mice

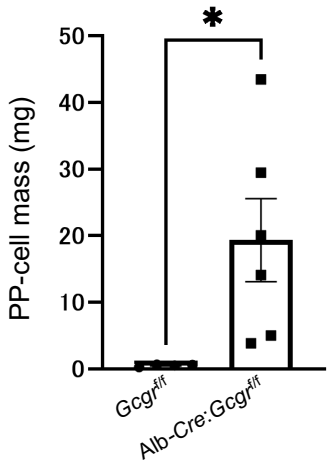

S2 Fig. PP-cell mass in in 40 week-old *Gcgr*$^{f/f}$ mice and Alb-*Cre*:*Gcgr*$^{f/f}$ mice

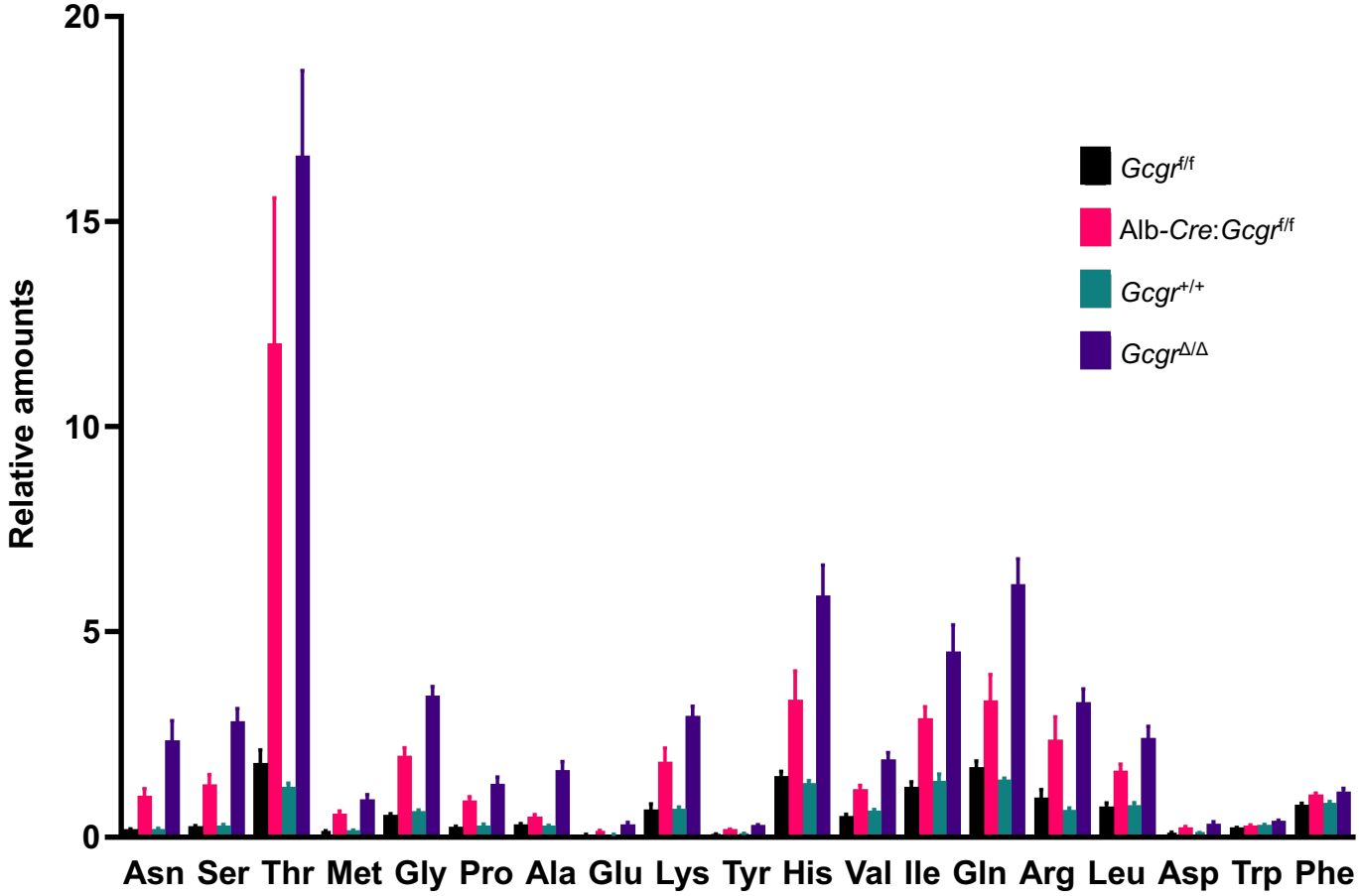

S3 Fig. Plasma levels of individual amino acids in 10 week-old *Gcgr*$^{f/f}$, Alb-*Cre*:*Gcgr*$^{f/f}$, *Gcgr*$^{+/+}$, and *Gcgr*$^{\Delta/\Delta}$ mice

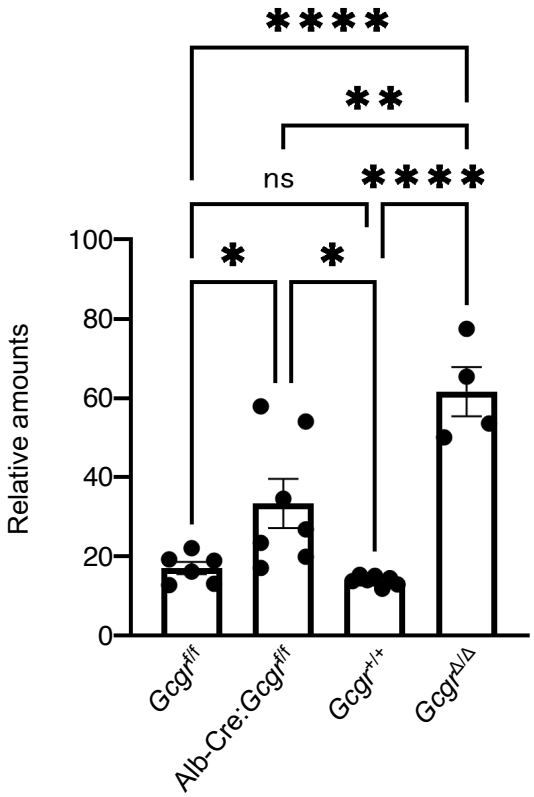

S4 Fig. Plasma glutamine levels in 10 week-old *Gcgr*$^{f/f}$, Alb-*Cre*:*Gcgr*$^{f/f}$, *Gcgr*$^{+/+}$, and *Gcgr*$^{\Delta/\Delta}$ mice

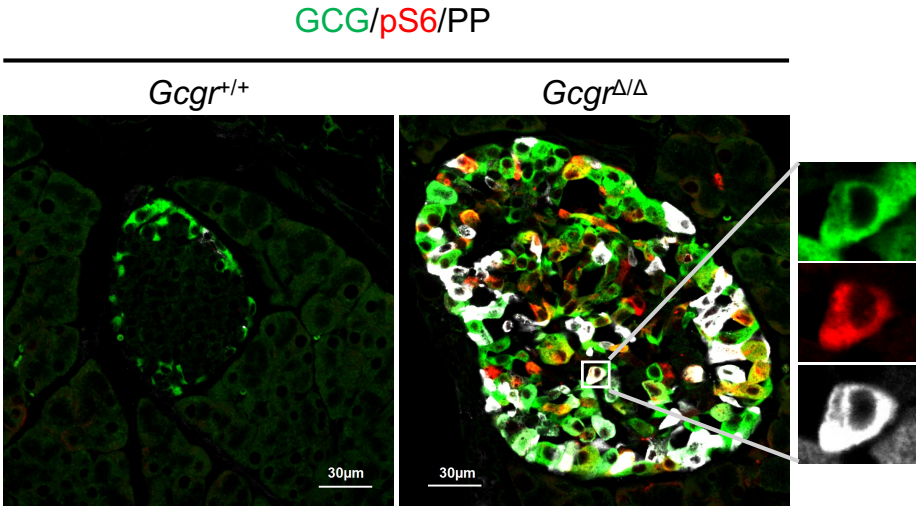

S5 Fig. Activation of the mTOR pathway in GCG^{+} PP^{+} cells from 40 week-old *Gcgr*$^{+/+}$ mice and *Gcgr*$^{\Delta/\Delta}$ mice

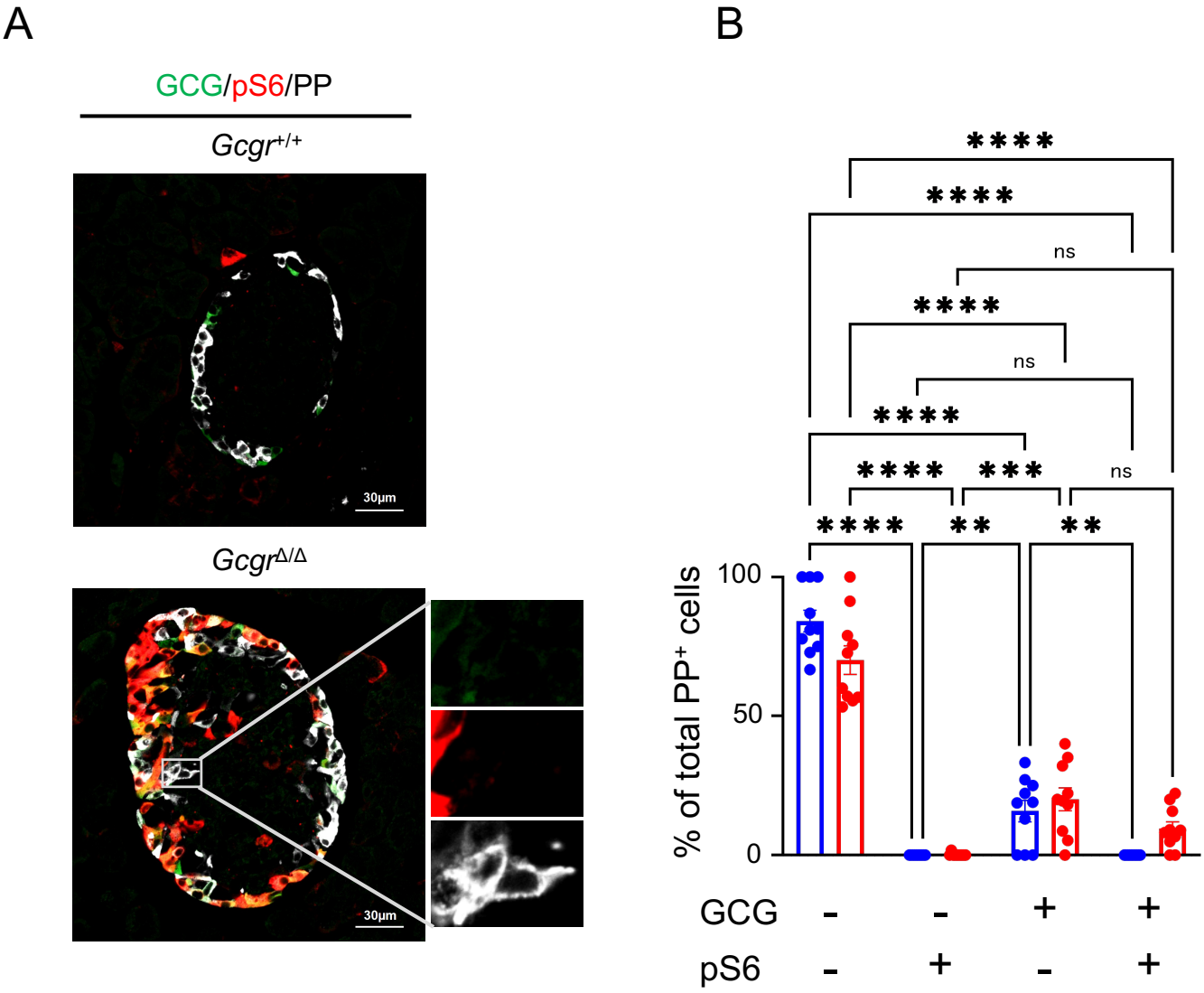

S6 Fig. Comparison of the number of PP^{+} positive-cells based on the presence or absence of glucagon and pS6 signals in 4 week-old *Gcgr*$^{+/+}$ mice and *Gcgr*$^{\Delta/\Delta}$ mice